Vibrational Predissociation Dynamics of He−I_2(B) Mediated by Orbiting Resonances[†]

A. García-Vela*

Instituto de Física Fundamental, C.S.I.C., Serrano 123, 28006 Madrid, Spain

Received: December 4, 2008; Revised Manuscript Received: January 21, 2009

The He−I_2(B, v) resonances embedded in the continuum of the $v = 60$ and 59 vibrational manifolds are investigated. Such states manifest a nature of overlapping and long-lived orbiting resonances, which are supported by centrifugal barriers originated in internal rotational excitation of I_2 and He within the complex. The same number of orbiting resonances, six, is found for $v = 60$ and for $v = 59$, with similar energy positions and wave functions, indicating that the spectrum of orbiting resonances changes slowly with the vibrational state v. Three of the orbiting resonances appear at nearly the same energies as the peaks observed experimentally in the vibrational relaxation cross section of I_2(B, $v = 21$) through low temperature collisions with He. Such finding suggests that the cross section peaks have their origin in orbiting resonances of the He−I_2(B, $v = 21$) complex formed upon the collision.

I. Introduction

The spectroscopy and dynamics of van der Waals (vdW) rare-gas clusters doped with molecular impurities have been extensively studied during the last three decades.[1−24] Among these studies, the pioneering theoretical works of Benny Gerber and co-workers contributed remarkably to the progress of the field.[25−28] As a result of this extensive research, the behavior of these clusters is, at present, well understood in general. There are, however, some aspects that still require further detailed investigation. One such aspect is the presence in vdW clusters of orbiting resonances embedded in the continuum, and the role they play in the cluster photofragmentation dynamics when such resonances are accessible.

Signature of these resonances has been found in different processes involving vdW clusters. Among them is the He−ICl(B, v') complex, where metastable intermolecular states of the type of orbiting resonances were observed spectroscopically.[29] Those states lie just above the He+ICl(B, $v' = 2, j' = 0$) dissociation threshold but are trapped behind a centrifugal barrier due to orbital motion of He around ICl.

The role of long-lived orbiting resonances was also invoked to explain some unexpected findings observed experimentally in the vibrational predissociation of the Ne−Br_2(B, v') vdW complex. These findings were Br_2 product rotational distributions more excited than expected,[20] and significantly longer than expected appearance times of the Br_2 products.[30] Theoretical simulations (classical and quantum mechanical ones) suggested that the above experimental findings were originated by intramolecular vibrational redistribution (IVR) mechanisms, where the resonances embedded in the continuum played the role of long-lived intermediate states in which the complex was temporarily trapped before dissociation.[20,21,31,32] More recently, the Ne−Br_2(B, $v = 26$) continuum resonances were characterized, confirming their nature of long-lived orbiting resonances supported by centrifugal barriers originated in rotational excitation of Br_2 and Ne within the complex.[33] The resonances were found to be strongly overlapping and highly delocalized in space. It is noted that in this case the orbiting resonances are supported by centrifugal barriers associated with the internal rotation of the Br_2 and Ne subunits within the complex (with internal angular momenta j and l, respectively, in Jacobi coordinates). This is a different situation from the more common one where the orbiting resonances are supported by a centrifugal barrier associated with the total angular momentum of the system, J.

Orbiting resonances present in the He−I_2 vdW complex have also been suggested as responsible for the enhancement at certain energies of the collision-induced vibrational relaxation cross section of I_2 through collisions with He at low temperatures.[34−38] In the most recent experiments,[37,38] the vibrational relaxation of I_2(B, $v' = 21$) by collisions with He was investigated in the energy range 0.65−5.8 cm^{-1}. The vibrational relaxation cross section measured exhibited a pattern of peaks and nodes consisting of three peaks appearing at energies smaller than 2 cm^{-1}. The origin of the cross section peaks was attributed to continuum resonances of the He−I_2(B, $v' = 21$) complex, which is formed upon the low energy collisions, and that enhance the I_2(B, $v' = 21$) vibrational relaxation probability.

The aim of the present work is to investigate the continuum resonances of the He−I_2(B) cluster. Theoretical evidence of IVR mechanisms mediated by continuum resonances has been found in the vibrational predissociation of He−I_2(B).[39] The goal here is 2-fold. On the one hand, it is intended to explore the nature of the He−I_2(B) continuum resonances to asses whether they are orbiting resonances of the same type as those found in the case of Ne−Br_2(B).[33] On the other hand, it is pursued to analyze whether the resonances found can explain the origin of the cross section enhancement observed experimentally.[37,38] Similarly as in the case of Ne−Br_2(B),[33] in this work the continuum resonances of He−I_2(B) are accessed and probed by simulating the vibrational predissociation of the complex, instead of the He+I_2(B) collisional process investigated experimentally.[37,38]

This Article is organized as follows. Section II presents the methodology used and the computational details. The results are presented and discussed in section III. Conclusions are given in section IV.

II. Theoretical Method

It has been shown in the case of Ne−Br_2(B) that by exciting a Rg−X_2(B) complex (Rg = rare gas atom, X = halogen atom)

[†] Part of the "Robert Benny Gerber Festschrift".

* Corresponding author. E-mail: garciavela@imaff.cfmac.csic.es.

10.1021/jp8106759 CCC: $40.75
Published on Web 03/02/2009

to a given intermolecular resonance state corresponding to a sufficiently high vibrational manifold v' of the $X_2(B)$ moiety, the excited resonance can interact with the nearby resonances embedded in the continuum of the $v' - 1$ manifold, and thus they can be accessed and probed.[32] If the ground intermolecular resonance (for instance) of Rg−$X_2(B, v')$ is initially excited, vibrational predissociation of the complex takes place populating the $v' - 1$ vibrational manifold (and lower ones). When the initial Rg−$X_2(B, v')$ ground intermolecular resonance is coupled to $v' - 1$ continuum resonances, these latter resonances are populated in the predissociation process (giving rise to IVR effects) and can be probed. Let us denote by v_c the Rg−$X_2(B)$ vibrational level such that for $v' \geq v_c$ the $\Delta v' = -1$ channel of vibrational predissociation is energetically closed. The situation in which the Rg−$X_2(B, v')$ initial ground intermolecular resonance is closer in energy to the Rg−$X_2(B, v' - 1)$ continuum resonances is usually achieved for the v' levels near v_c and just below it (typically for $v' = v_c - 1$, $v_c - 2$, and for some systems also $v' = v_c$). Thus, those initial v' levels are the optimal ones to access and probe the $v' - 1$ continuum resonances in a vibrational predissociation process of Rg−$X_2(B)$.

In the case of He−$I_2(B)$ with the potential-energy surface used in this work, the vibrational level v_c for which the $\Delta v' = -1$ dissociation channel becomes energetically closed is $v_c = 62$. Thus, the ground intermolecular resonances of He−$I_2(B, v')$ for $v' = 61$ and 60 are well-suited initial states to probe the He−$I_2(B, v'-1)$ continuum resonances, because they are energetically located 0.78 cm^{-1} above the He+$I_2(B, v' - 1 = 60, j' = 0)$ dissociation limit and 2.21 cm^{-1} above the He+$I_2(B, v' - 1 = 59, j' = 0)$ dissociation limit, respectively. Therefore, simulations of the He−$I_2(B, v')$ vibrational predissociation dynamics have been carried out for the two initial states, the ground intermolecular resonance of He−$I_2(B, v')$ for $v' = 61$ and 60. In this way, the He−$I_2(B, v'-1)$ continuum resonances associated with two different vibrational levels, $v'-1 = 60$ and 59, can be investigated and compared. It is noted that the continuum resonances associated with the $v' - 1 = 21$ level (the vibrational level studied experimentally) cannot be accessed and probed through a vibrational predissociation process starting from the ground intermolecular resonance of He−$I_2(B, v' = 22)$. The reason is that for these low v' levels, there are no IVR effects in He−$I_2(B, v')$, because the initial ground intermolecular resonance of He−$I_2(B, v' = 22)$ is located at a high enough energy relative to the $v' - 1 = 21$ continuum resonances as to make the coupling and interaction between the initial and the continuum resonances negligible.

The system is represented in Jacobi coordinates (r, R, θ), were r is the I−I internuclear distance, R is the separation between He and the I_2 center-of-mass, and θ is the angle between the r and R vectors. The potential-energy surface used to model the interaction of the He−$I_2(B)$ complex is an empirical one, which has been described in detail elsewhere.[40] This potential surface was modeled as a sum of pairwise He−I Morse interactions plus a three-body interaction term with an explicit dependence on the I−I internuclear separation. The parameters of the potential function were fitted to reproduce the available spectroscopic and dynamical experimental data (spectral blueshifts and vibrational predissociation lifetimes) in a wide range, $v' = 10-67$, of vibrational excitations of He−$I_2(B)$. The experimental data are reproduced by the fitted potential surface with good agreement across the $v' = 10-67$ range, and particularly for high v' levels, which was attributed to the three-body interaction term included in the potential.[40] Thus, the potential surface of ref 40 is particularly well suited for the simulations of the He−$I_2(B, v')$ vibrational predissociation for the high $v' = 61$ and 60 initial levels carried out in this work. It is noted that an ab initio potential surface for the He−$I_2(B)$ system has been recently reported.[41] However, as pointed out in ref 41, the range of I_2 internuclear separations spanned by the ab initio potential is $r = 2.65-3.45$ Å, implying that only the few first vibrational excitations v' of He−$I_2(B, v')$ can be accurately described. Therefore, the choice of the empirical potential of ref 40 appears more suitable for such high v' levels as those studied here.

The vibrational predissociation process starting from the ground intermolecular resonance of He−$I_2(B, v' = 61, 60)$ was simulated by means of a wave packet method.[31,32] The wave packet representing the system is expanded as

$$\Phi(r, R, \theta, t) = \sum_{vj} C_{v,j}(R, t)\chi_v^{(j)}(r)P_j(\theta)e^{-iE_v^{(j)}t/\hbar} \qquad (1)$$

where $\chi_v^{(j)}(r)$ and $E_v^{(j)}$ are the rovibrational eigenvectors and eigenenergies of $I_2(B)$, respectively, $P_j(\theta)$ are normalized Legendre polynomials, and $C_{v,j}(R, t)$ are the expansion coefficients, which are propagated through a set of time-dependent coupled equations. The basis set used consisted of 20 rotational states (with even j) and six vibrational states ($v = v', v' - 1,..., v' - 5$). The $C_{v,j}(R, t)$ coefficients are represented on a grid in R consisting of 3600 equidistant points with $R_{in} = 0a_0$ and $\Delta R = 0.25a_0$. The wave packet is absorbed at the edges of the grid by multiplying each $C_{v,j}(R, t)$ packet by the function $\exp[-a(R-R_{abs})^2]$, with $a = 0.0025a_0^{-2}$ and $R_{abs} = 850.0a_0$. This large grid in R is used to avoid the need to absorb the wave packet components associated with the $v' - 1$ continuum resonances. The components of these resonances, and especially those of the lowest ones, are particularly difficult to absorb, because the resonances appear at very low energies (with respect to the $v' - 1$ dissociation threshold) and therefore have associated very large de Broglie wavelengths. In this sense, the strategy adopted here has been to perturb the resonances under study in the least way possible with an artificial procedure like wave packet absorption. An absorbing potential is useful, however, to absorb the $v < v' - 1$ wave packet components, which have larger energies and smaller de Broglie wavelengths. Zero total angular momentum is assumed for the system.

The wave packet was propagated until $t_f = 400$ ps, and by Fourier transforming its autocorrelation function, the excitation spectrum corresponding to the $v' = 61$ and 60 initial states was obtained. This long time propagation ensures convergence of the calculated spectra.

III. Results and Discussion

A. Excitation Spectra and Resonance Energies and Widths. Before discussing the results, it is useful to give the energy locations of some of the states involved in the process under study. The $E_v^{(j=0)}$ energies corresponding to the He+$I_2(B, v, j = 0)$ dissociation threshold for $v = 59$, 60, and 61 are −136.90, −120.99, and −106.38 cm^{-1}, respectively ($E_v^{(j=0)} = 0$ corresponds to separated I atoms). In addition, the He−$I_2(B, v)$ intermolecular resonance states lying energetically below the He+$I_2(B, v, j = 0)$ dissociation threshold have been calculated variationally[39] for $v = 59$, 60, and 61. The resonance energies obtained are collected in Table 1. The $m = 0$ resonance in the cases of $v = 61$ and 60 is the initial state from which vibrational predissociation of He−$I_2(B)$ takes place in this study.

The calculated excitation spectra of He−$I_2(B, v')$ for $v' = 61$ and 60 are shown in Figures 1 and 2, respectively. In both cases,

TABLE 1: Calculated He−I_2(B, v) Resonance Energies Relative to the He+I_2(B, v, $j = 0$) Dissociation Limit

	$E_m^{(v)}$ (cm^{-1})		
m	$v = 59$	$v = 60$	$v = 61$
0	−13.579	−13.700	−13.834
1	−6.229	−6.154	−6.072
2	−4.818	−4.723	−4.623
3	−3.290	−3.282	−3.272
4	−1.293	−1.359	−1.429
5	−0.078	−0.074	−0.067

most of the spectral intensity appears at energies above the He+I_2(B, $v' - 1, j' = 0$) dissociation threshold, that is, in the continuum of the $v'-1$ vibrational manifold. In this region, the two spectra exhibit a big peak with a shape that is far from being Lorentzian. In the energy region below the $v' - 1$ dissociation threshold, the spectra show three overlapping features, which, as we shall see below, can be identified as associated with the three highest $m = 3-5$ intermolecular resonances of He−I_2(B, $v' - 1$) located energetically below the $v' - 1$ dissociation limit.

To identify the energy positions and widths of the resonances contributing to the spectra, they were fitted to a sum of weigthed Lorentzian line shapes. The fits to the spectra are also shown in Figures 1 and 2, along with the weighted Lorentzian line shapes used in the fits. The fit is quite good for both spectra, indicating that the assignment of resonances made is reliable enough. The assigned resonance energies and widths for the spectra of $v' = 61$ and 60 are presented in Tables 2 and 3, respectively.

As already anticipated, the three features of the spectra appearing at energies below the $v' - 1$ dissociation threshold are assigned to the three highest $m = 3-5$ resonances of the $v' - 1$ manifold. In the second column of Tables 2 and 3, the three resonance energies obtained from the fits to the spectra are listed, while in the fourth column the same resonance energies are presented, but now relative to the energy $E_{v'-1}^{(j'=0)}$ of the $v' - 1$ dissociation threshold. These latter energies are very close to the corresponding resonance energies of Table 1 calculated variationally.

In both spectra, the big peak at energies above the $v' - 1$ threshold cannot be fitted by a single Lorentzian line shape. Actually this peak turns out to be a superposition of several overlapping Lorentzian line shapes associated with continuum resonances. Up to six resonances ($n = 0-5$) have been identified in this region, in an energy range of about 6 cm^{-1}. Figures 1 and 2 show a regime of strongly overlapping resonances embedded in the $v' - 1$ continuum. This situation is very similar to that found in the case of Ne−Br_2(B, $v' - 1 = 26$).[33]

Tables 2 and 3 show that the $v' - 1$ continuum resonances are long-lived states, with lifetimes ranging from ∼4 to ∼30 ps. The resonance widths of the continuum resonances are found to increase monotonically with increasing resonance energy. The separation between adjacent resonances $E_n^{res} - E_{n-1}^{res}$ increases with increasing resonance energy as well. These trends for the resonance width and energy separation between adjacent resonances are characteristic of orbiting resonances supported by centrifugal barriers. Indeed, the energy of an orbiting resonance depends on the magnitude of the centrifugal barrier as $j(j + 1)\hbar^2$, with j being the angular momentum associated with the internal rotation of He or I_2 within the He−I_2 complex (because the total angular momentum of the complex is $J = 0$, the internal angular momenta of both He and I_2 must coincide in magnitude and have opposite sign). As the magnitude of the internal rotation, and therefore of j, increases, the energy of the orbiting resonance will increase as roughly the square of j, causing a quadratic increase of the energy separation between adjacent resonances. Similarly, as the resonance energy increases, the orbiting resonance becomes closer to the top of the centrifugal barrier, leading to a larger width and a faster decay of the resonance. The nature of the present orbiting resonances of He−I_2(B) would be similar to the continuum resonances detected spectroscopically for He−ICl(B, $v' = 2$).[29]

It is noted that the energies and widths of the $v' - 1$ continuum resonances found for $v' = 61$ and 60 are very similar. Taking into account that the two spectra of Figures 1 and 2 have a different shape, this result provides strong support to the fits carried out and to the assignments obtained from them. This finding would suggest that the spectrum of continuum resonances is very similar for the different vibrational manifolds v of He−I_2(B, v) and that only rather small changes take place in that spectrum as v increases. This behavior of the spectrum of continuum resonances with v would not be very much surprising, because it is actually the same behavior shown by the spectrum of He−I_2(B, v) intermolecular resonances lying energetically below the He+I_2(B, $v, j = 0$) dissociation threshold. The changes with v in the spectrum of He−I_2(B, v) resonances lying both above and below the v dissociation threshold are directly related to the changes of the He−I_2(B, v) vdW interaction, which changes rather slowly with v. This point will be analyzed in more detail below.

In the vibrational relaxation cross section measured in the He+I_2(B, $v' = 21$) low-energy collision experiments,[37,38] three peaks were found at the energies 0.82, 1.17, and 1.67 cm^{-1}. Such peaks were attributed to intermolecular resonances of the He−I_2(B, $v' = 21$) vdW complex formed upon the collision. These resonances would be embedded in the He+I_2(B, $v' = 21$) continuum. Most interestingly, Tables 2 and 3 show that three of the continuum resonances found for $v' - 1 = 60$ and 59, those labeled as $n = 1$, 2, and 3, have energies very close to those of the cross section peaks observed experimentally. In addition, it is noted that the width of the cross section peaks increases with energy, as does the width of the resonances found in this work.

In principle, the $v' = 21$ vibrational manifold involved in the experiments seems to be quite different from the $v' - 1 = 60$ and 59 manifolds involved in the present calculations, and in this sense caution should be exerted in comparing the current results with the experimental findings. Nonetheless, the qualitative result is that the present simulations for He−I_2(B, $v' = 61, 60$) find a group of continuum resonances in the same low-energy region, $E < 7$ cm^{-1}, where He+I_2(B, $v' = 21$) collisional experiments detect peaks in the vibrational relaxation cross section. It seems unlikely that both the experimental and the theoretical results are unrelated. It appears more likely that the He+I_2(B, v') vdW interaction for $v' = 21$ is rather similar to the interaction for $v' = 61$ and 60 as to give rise to similar spectra of intermolecular resonances. This is supported theoretically by the result that the energy position of the $m = 0$ ground resonance state for $v' = 21$ is −13.834 cm^{-1},[40] very similar to the $m = 0$ position for $v' = 61, 60$ (see Table 1). It is also supported experimentally by the similarity of the spectral blueshifts observed for $v' = 21$ [3.80 ± 0.02 cm^{-1} (refs 2 and 42) or 3.79 ± 0.05 cm^{-1} (ref 43)] and that measured for $v' = 61$ (3.77 ± 0.05 cm^{-1}).[43] Thus, it appears that the He−I_2(B, v') vdW interaction for $v' = 21$ is similar enough to that in the region near $v' = 61$ as to support similar spectra of continuum resonances.

In the present calculations, six continuum resonances were identified for $v'-1 = 60, 59$, while in the relaxation cross section measured for $v' = 21$ only three peaks were found. Again, this

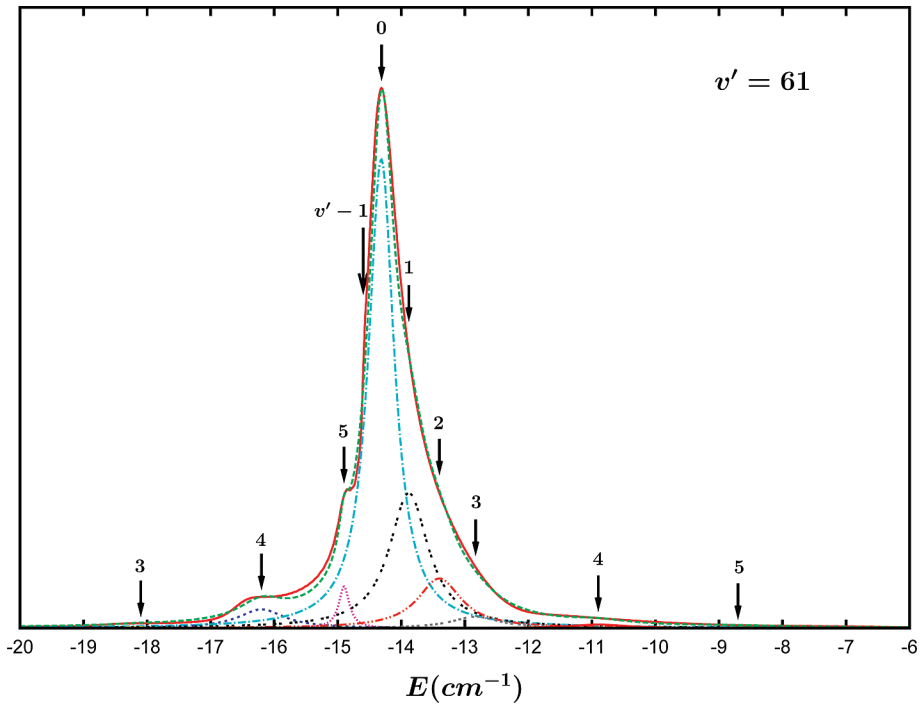

Figure 1. Calculated excitation spectrum from the ground intermolecular vdW resonance of He−$I_2(B, v' = 61)$ (red solid line), fitted spectrum as a sum of weighted Lorentzian line shapes (green dashed line), and the different Lorentzian line shapes used in the fit. The energy axis is relative to the He+$I_2(B, v' = 61, j' = 0)$ dissociation threshold. The arrow labeled by $v'-1$ indicates the He+$I_2(B, v' - 1 = 60, j' = 0)$ dissociation threshold. The arrows to the right of the $v' - 1$ limit and labeled by the numbers $n = 0-5$ indicate the position of the identified $v' - 1$ continuum resonances. The arrows to the left of the $v' - 1$ limit and labeled by the numbers $m = 3-5$ indicate the position of the identified resonances located below the $v' - 1$ dissociation limit.

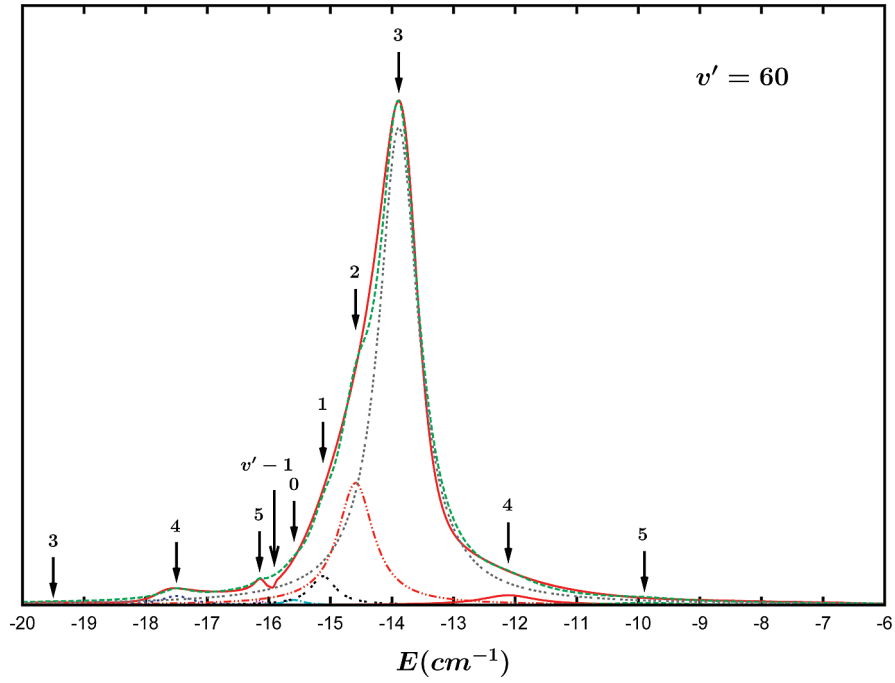

Figure 2. Same as Figure 1 but for the case of the initial ground vdW resonance of He−$I_2(B, v' = 60)$.

discrepancy might be due to possible deficiencies of the empirical potential surface used here and/or to larger differences than expected between the resonance spectra of $v' = 21$ and $v'-1 = 60, 59$. However, we should also note the following. On the one hand, the experiment did not probe the energy region $E < 0.65$ cm^{-1} where the $n = 0$ continuum resonance appears. On the other hand, in the energy range $E = 2-6$ cm^{-1}, there are only five measurements of the vibrational relaxation cross section,[37] and if the possible peaks associated with the resonances $n = 4$ and 5 are rather weak (as they are expected to be), the possibility that they might have been missed in the measured cross section should be considered. So the present results might not yet be in discrepancy with the experimental ones.

B. Distributions of the Resonance Wave Functions. After the energy positions of the $v' - 1$ continuum resonances were identified in the spectra of $v' = 61$ and 60, the associated resonance wave functions were obtained by Fourier transform of the wave packet of eq 1 from the time to the energy domain

TABLE 2: Resonance Energies E_k^{res} and Widths Γ (Full Width at Half Maximum) Obtained from the Fit to the Spectrum of Figure 1[a]

$k = m/n$	E_k^{res} (cm^{-1})	$E_k^{res} - E_{k-1}^{res}$ (cm^{-1})	$E_k^{res} - E_{v'-1}^{(j'=0)}$ (cm^{-1})	Γ (cm^{-1})	τ (ps)
3	−18.10		−3.50	1.00	5.31
4	−16.20	1.90	−1.60	0.88	6.03
5	−14.90	1.30	−0.30	0.20	26.54
0	−14.31	0.29	0.29	0.49	10.83
1	−13.88	0.43	0.72(0.82)	0.75	7.08
2	−13.40	0.48	1.20(1.17)	0.83	6.40
3	−12.83	0.57	1.77(1.67)	0.91	5.83
4	−10.90	1.93	3.70	1.08	4.92
5	−8.70	2.20	5.90	1.30	4.08

[a] When $k = m = 3-5$, the resonance corresponds to states located below the He + $I_2(B, v' - 1, j' = 0)$ dissociation threshold, while when $k = n = 0-5$, the resonances correspond to $v' - 1 = 60$ continuum resonances located above the He + $I_2(B, v' - 1, j' = 0)$ dissociation limit. Lifetimes τ corresponding to the resonance widths, energy separations between adjacent resonances (third column), and energy separations between each resonance and the $v' - 1$ dissociation threshold (fourth column) are also listed. The numbers in parentheses in the fourth column correspond to the positions of the cross sections peaks found experimentally in ref 37. In the case of $k = n = 0$ in the third column, the energy separation is relative to the $v' - 1$ dissociation threshold.

TABLE 3: Same as Table *2* but for the Case of the $v' - 1 = 59$ Resonances

$k = m/n$	E_k^{res} (cm^{-1})	$E_k^{res} - E_{k-1}^{res}$ (cm^{-1})	$E_k^{res} - E_{v'-1}^{(j'=0)}$ (cm^{-1})	Γ (cm^{-1})	τ (ps)
3	−19.50		−3.59	0.98	5.42
4	−17.50	2.00	−1.59	0.60	8.85
5	−16.15	1.35	−0.24	0.17	31.23
0	−15.59	0.32	0.32	0.38	13.97
1	−15.12	0.47	0.79(0.82)	0.50	10.62
2	−14.59	0.53	1.32(1.17)	0.70	7.58
3	−13.89	0.70	2.02(1.67)	0.78	6.81
4	−12.11	1.78	3.80	1.10	4.83
5	−9.90	2.21	6.01	1.35	3.93

for the resonance energies of Tables 1 and 2.[44] For each energy E_n^{res}, the components of the wave packet obtained in the different vibrational manifolds v were analyzed. A typical example of the radial distributions found is shown in Figure 3, for the case of the energy associated with the resonance $n = 1$ embedded in the $v' - 1 = 60$ continuum.

The radial distribution found for the $v = v'$ component of the wave packet (upper panel of Figure 3) coincides with the corresponding radial distributions of the initial ground vdW resonance state of He−$I_2(B, v' = 61, 60)$. This is so for all of the E_n^{res} energies associated with the different continuum resonances. Actually this result was expected, because the $v = v'$ component of the time-dependent wave packet is composed only of the initial ground resonance state of the He−$I_2(B, v')$ complex. The $v = v'$ radial distribution peaks around $7a_0$, and it is rather localized between 5 and $11a_0$. The good coincidence between the radial distribution of the initial resonance state of the complex and the $v = v'$ distribution found by time to energy Fourier transform of the wave packet is an indication of the good quality of the energy-selected wave functions obtained through Fourier transform of the wave packet propagated for 400 ps.

The radial distribution associated with the $v = v' - 1$ component of the wave packet has a structure with several clear peaks (medium panel of Figure 3). The $v' - 1$ radial distributions exhibit a main peak around $R = 14a_0$, which is significantly

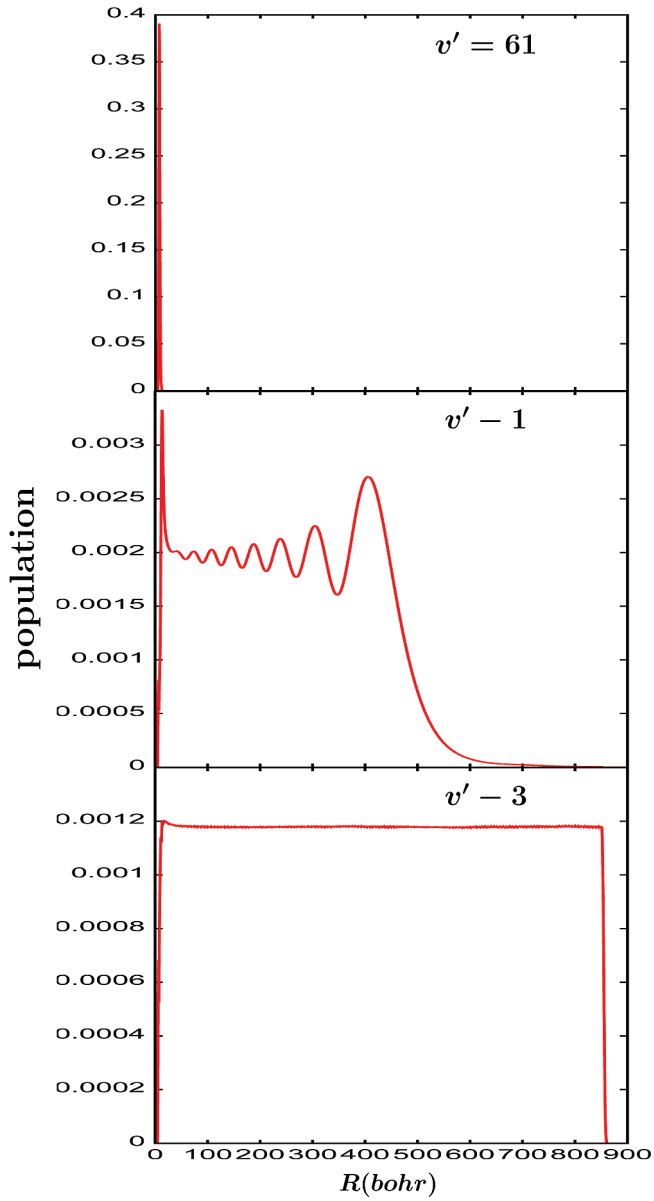

Figure 3. Radial distributions obtained in three different vibrational manifolds (v', $v' - 1$, and $v' - 3$) by Fourier transform of the wave packet propagated from the He−$I_2(B, v' = 61)$ initial state at the energy $E_{n=1}^{res} = -13.88\ cm^{-1}$ of the $n = 1$, $v' - 1 = 60$ continuum resonance.

shifted and extended in the interaction region with respect to the $v = v'$ distribution. A series of peaks at larger distances is also displayed in the radial distribution. The spreading of the $v' - 1$ radial distribution depends on the E_n^{res} energy. As E_n^{res} increases, both the radial spreading and the number of peaks in the structure increase as well. This is the result that the $v' - 1$ continuum resonances undergo tunneling through the centrifugal barrier that supports the resonances. As the resonance energy increases and the resonance position becomes far away from the bottom of the centrifugal barrier, the tunneling rate of the resonances increases. Thus, for a given propagation time (like $t_f = 400$ ps), the radial spreading within the wave packet of the $v' - 1$ resonances with a higher tunneling rate will be larger.

The $v < v' - 1$ components of the wave packet (lower panel of Figure 3) found for all of the resonance energies are all similar, exhibiting no structure and a constant value for R distances outside the interaction region. The shape of the radial distributions is consistent with that of distributions of continuum

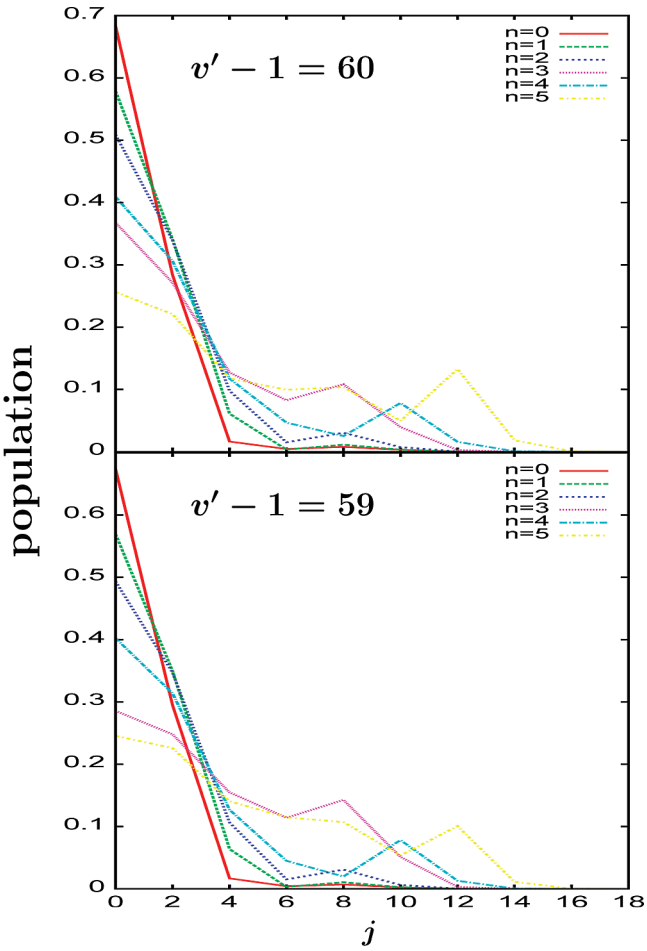

Figure 4. Free-rotor distributions associated with the wave functions of the six identified continuum resonances of $v' - 1 = 60$ (upper panel) and $v' - 1 = 59$ (lower panel). All of the distributions are normalized to unity.

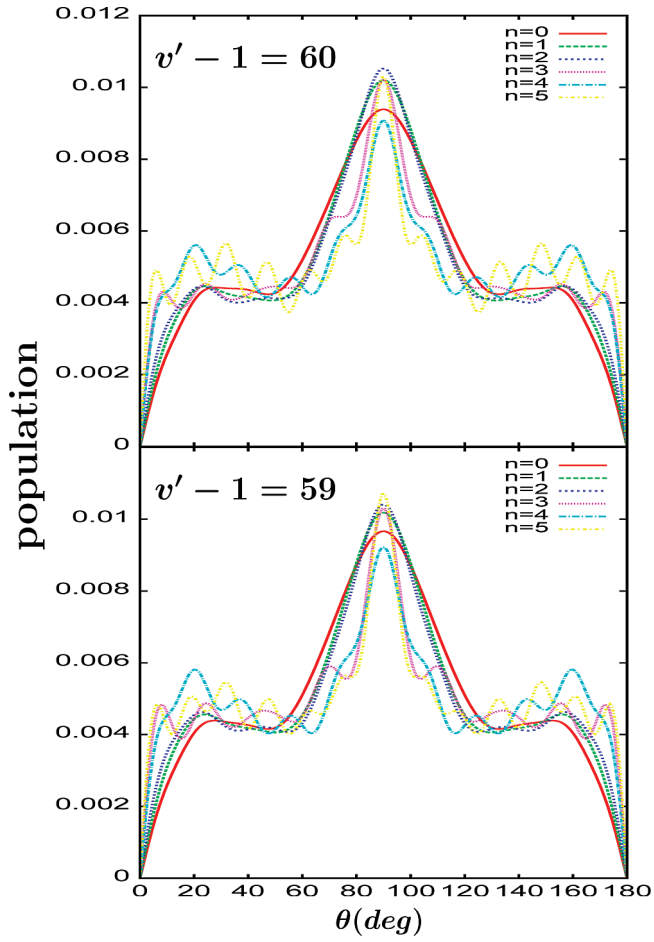

Figure 5. Angular distributions associated with the wave functions of the six identified continuum resonances of $v' - 1 = 60$ (upper panel) and $v' - 1 = 59$ (lower panel). All of the distributions are multiplied by the sin θ factor contained in the volume element in Jacobi coordinates and normalized to unity.

states corresponding to the fragments $I_2(B, v < v' - 1, j)$+He. Indeed, in such $v < v' - 1$ continuum states, the relative motion of the two fragments in the dissociative R coordinate is described by a plane wave e^{ikR} (where k depends on the energy of the final rovibrational state of the $I_2(B, v < v' - 1, j)$ fragment), and the square of a plane wave is a constant function of R. The distribution associated with each $v < v' - 1$ wave packet component consists of a superposition of a few $I_2(B, v < v' - 1, j)$+He continuum states, that is, a few plane waves in the R coordinate, that leads to an essentially constant radial distribution like that shown in the lower panel of Figure 3. The $v < v' - 1$ continuum states can be populated both by direct predissociation from the initial He−$I_2(B, v')$ state and by indirect predissociation from the $v' - 1$ continuum resonances acting as intermediate states after they are accessed from the initial state.

In the following, we shall focus on the analysis of the wave functions obtained for the $v' - 1$ continuum resonances. In this sense, the free-rotor and angular distributions associated with the resonance wave functions provide interesting information about the nature of the resonances. Those distributions are shown in Figures 4 and 5 for all of the continuum resonance wave functions of $v' - 1 = 60$ and 59.

The most interesting trend of the distributions of Figure 4 is that rotational excitation increases with increasing resonance energy. This indicates that the rotational barriers supporting the continuum resonances become increasingly higher as n grows. High rotational states up to $j \approx 16$ are populated in the resonance wave function distributions of the two $v' - 1$ manifolds investigated. The behavior of the free-rotor distributions of Figure 4 is consistent with the nature of the $v' - 1$ continuum states under study as orbiting resonances supported by centrifugal barriers originated by high rotational excitation of I_2 and He within the vdW complex.

The angular distributions (Figure 5) associated with the $v' - 1$ continuum resonance wave functions spread over all of the angular space, displaying most of their intensity around the perpendicular ($\theta = 90°$) and linear configurations ($\theta = 0°$ and $\theta = 180°$; the distributions of Figure 5 are multiplied by the sin θ factor contained in the volume element in Jacobi coordinates, and this factor damps the peaks of intensity appearing at $\theta = 0°$ and 180° in the distributions). For both $v' - 1 = 60$ and 59, the behavior found in the angular distributions is that the number of undulations increases with increasing n. This trend is consistent with the increase of rotational excitation with n found in the distributions of Figure 4.

From the above discussion in this section, it follows that the continuum resonances of He−$I_2(B)$ studied here are orbiting resonances supported by barriers originated by rotational excitation of I_2 and He within the vdW complex. Because these resonances seem to be the same as those detected experimentally in the He+$I_2(B, v' = 21)$ collisions,[37,38] the implication is that the resonances giving rise to the peaks found in the measured vibrational relaxation cross section would also be orbiting resonances. In addition, the behavior of the He−$I_2(B)$ orbiting

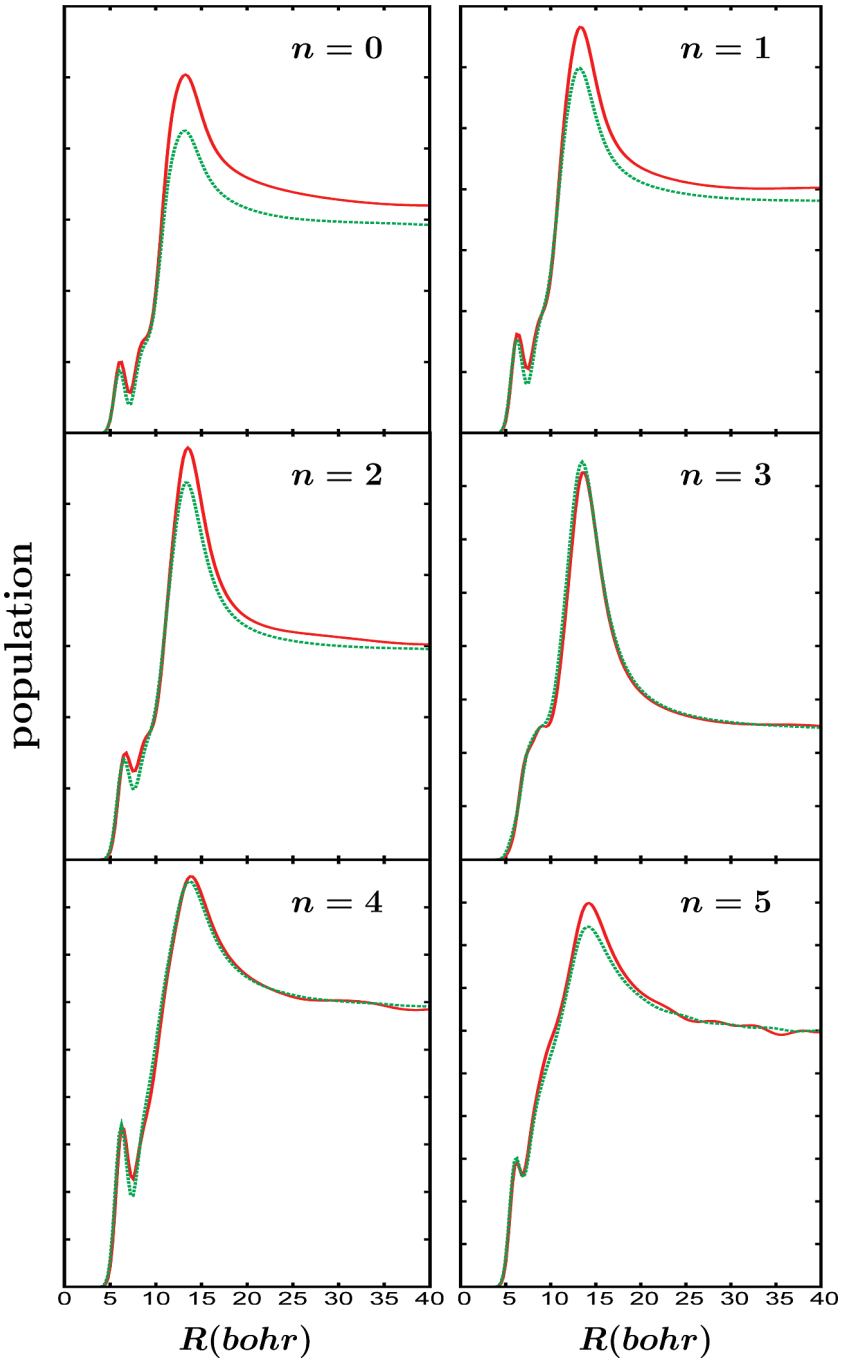

Figure 6. Comparison of the radial distributions associated with the wave functions of the $v' - 1 = 60$ (red solid lines) and $v' - 1 = 59$ (green dashed lines) continuum resonances.

resonances (regarding the trends of the resonance energies, widths, and wave function distributions with increasing n) is the same as the behavior found for the orbiting resonances in Ne−$Br_2(B)$. This similarity suggests that the presence of these orbiting resonances might be general to the whole family of rare gas−halogen vdW clusters, at least in the case of the Rg−X_2 triatomic complexes.

As already mentioned above, a most interesting point is to elucidate whether the spectrum of orbiting resonances changes rather little when the vibrational manifold v of He−$I_2(B, v)$ is changed, and if essentially the same orbiting resonances are found in the different v manifolds. The similarity of energy positions and widths of the orbiting resonances embedded in the continuum of $v' - 1 = 60$ and 59 (see Tables 2 and 3) points out in this direction. To analyze more closely whether the orbiting resonances found for both $v' - 1 = 60$ and 59 are actually the same resonance states, the associated resonance wave function distributions have been compared. Such comparisons are shown in Figures 6−8.

Figures 6−8 show that the wave function distributions in R, j, and θ associated with all of the orbiting resonances of $v' - 1 = 60$ and 59 display the same pattern of peaks and nodes. A very high similarity between the distributions of $v' - 1 = 60$ and 59 is typically found for all of the $n = 0$−5 resonances. Therefore, in addition to the energy positions and widths, the wave functions of the orbiting resonances of $v' - 1 = 60$ and 59 are also similar, meaning that actually we are dealing with the same resonance states in both vibrational manifolds. The implication is that the spectrum of continuum orbiting resonances seems to change slowly with v', as does the spec-

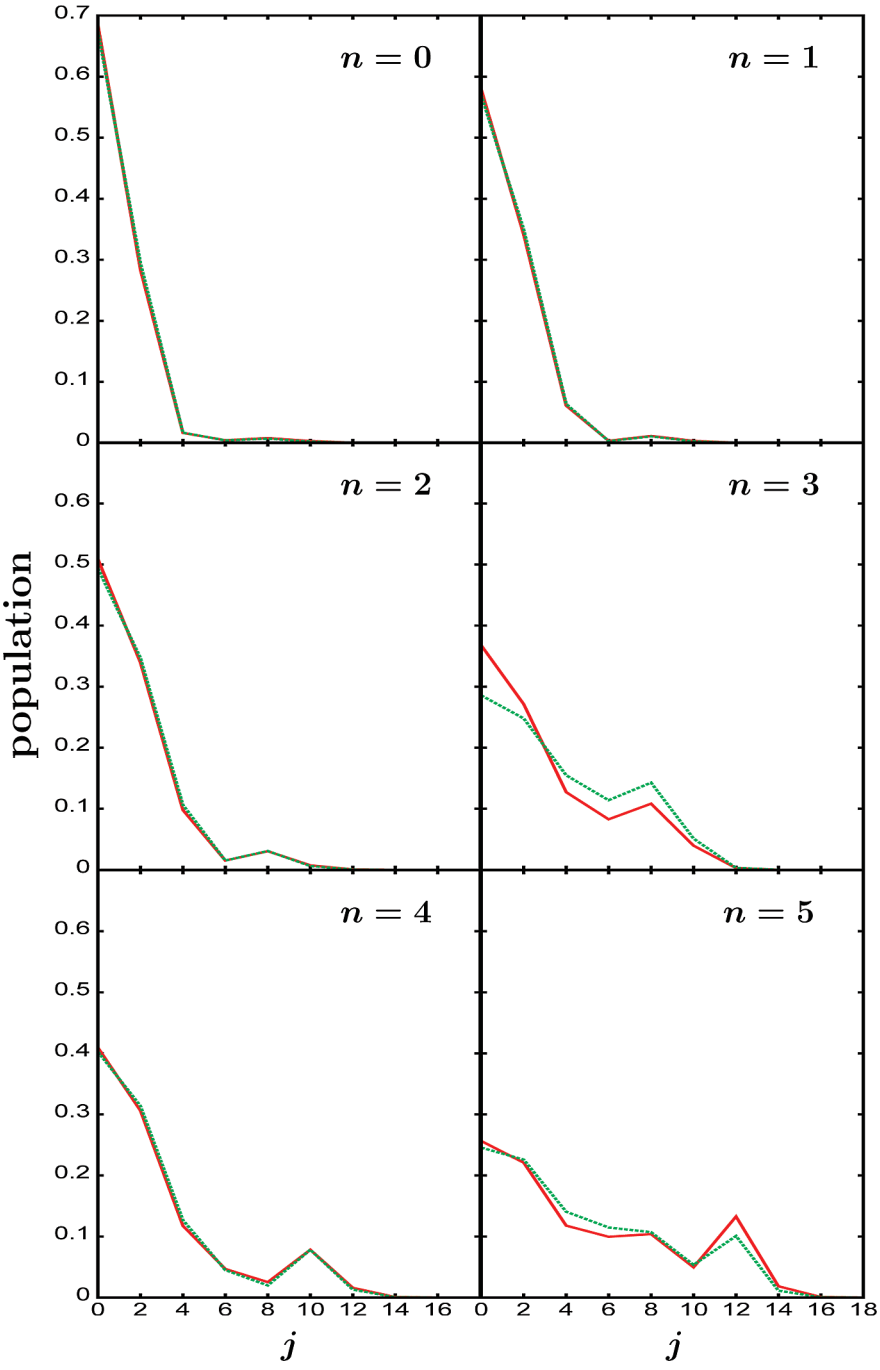

Figure 7. Same as in Figure 6 but for the free-rotor distributions. All of the distributions are normalized to unity.

trum of quasibound states located energetically below the He+$I_2(B, v')$ dissociation threshold.

It is interesting to note that in the interaction region displayed in Figure 6 the radial distributions are very similar for all of the continuum resonances. These distributions show that as n increases there is practically no excitation in the vdW stretching mode R. However, as mentioned above, this excitation takes place with increasing n in the angular (bending) mode, that is, in the internal rotation of the I_2 and He moieties within the complex, as shown by Figures 7 and 8.

IV. Conclusions

The He−$I_2(B, v)$ resonances embedded in the continuum of the $v = 60$ and 59 vibrational manifolds have been investigated. The continuum resonances found exhibit a nature of orbiting resonance states, supported by barriers originated in internal rotational excitation of I_2 and He within the vdW complex. Six orbiting resonances are identified in the two vibrational manifolds $v = 60$ and 59. Comparison of the energy positions, widths, and wave function distributions associated with the orbiting resonances of $v = 60$ and 59 shows that the same resonance states are supported in the two vibrational manifolds. It indicates that the spectrum of orbiting resonances changes slowly with v. Most interestingly, the energy positions of three of the orbiting resonances in both vibrational manifolds nearly coincide with the energies of the three peaks observed experimentally in the vibrational relaxation cross section of $I_2(B, v = 21)$ in low temperature collisions with He. This result would suggest that the peaks observed in the cross

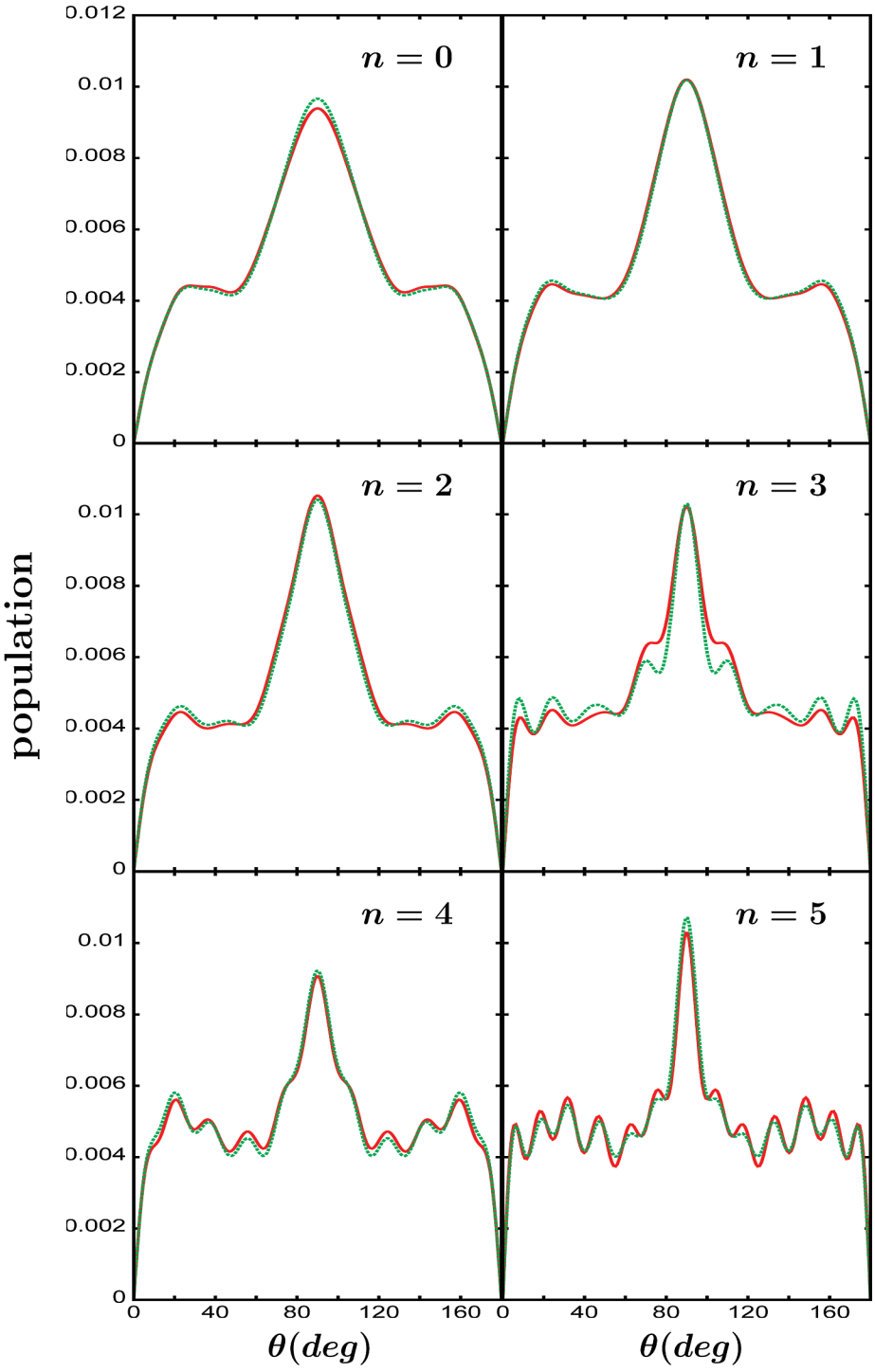

Figure 8. Same as in Figure 6 but for the angular distributions. All of the distributions are multiplied by the sin θ factor contained in the volume element in Jacobi coordinates and normalized to unity.

section are due to orbiting resonances of the He−I_2(B, v = 21) complex formed upon the collision.

The orbiting resonances found for He−I_2(B) exhibit the same behavior and characteristics as the orbiting resonances previously found for Ne−Br_2(B). This may suggest that the presence of orbiting resonances would be a general feature of (at least) triatomic rare gas−halogen vdW complexes. Investigation of this type of resonances on other vdW complexes should be very interesting.

Acknowledgment. This work was funded by C.I.CYT (Ministerio de Ciencia e Innovación), Spain, Grant No. FIS-2007-62002. The Red Espanola de Supercomputación (MareNostrum at BSC) and the Centro de Supercomputación de Galicia (CESGA) are acknowledged for the use of their computational resources.

References and Notes

(1) Sharfin, W.; Johnson, K. E.; Warton, L.; Levy, D. H. *J. Chem. Phys.* **1979**, *71*, 1292.
(2) Kenny, J. E.; Johnson, K. E.; Sharfin, W.; Levy, D. H. *J. Chem. Phys.* **1980**, *72*, 1109.
(3) Levy, D. H. *Adv. Chem. Phys.* **1981**, *47*, 323.
(4) van der Avoird, A.; Wormer, P. E. S.; Mulder, F.; Berns, R. M. *Top. Curr. Chem.* **1980**, *93*, 1.

(5) Beswick, J. A.; Jortner, J. *Chem. Phys. Lett.* **1977**, *49*, 13.
(6) Beswick, J. A.; Jortner, J. *Adv. Chem. Phys.* **1981**, *47*, 363.
(7) Swartz, B. A.; Brinza, D. E.; Western, C. M.; Janda, K. C. *J. Phys. Chem.* **1984**, *88*, 6272.
(8) Hair, S. R.; Cline, J. I.; Bieler, C. R.; Janda, K. C. *J. Chem. Phys.* **1989**, *90*, 2935.
(9) Drobits, J. C.; Lester, M. I. *J. Chem. Phys.* **1987**, *86*, 1662.
(10) García-Vela, A.; Villarreal, P.; Delgado-Barrio, G. *J. Chem. Phys.* **1990**, *92*, 6504.
(11) García-Vela, A.; Villarreal, P.; Delgado-Barrio, G. *J. Chem. Phys.* **1991**, *94*, 7868.
(12) Zhang, D. H.; Zhang, J. Z. H. *J. Chem. Phys.* **1991**, *95*, 6449.
(13) Gray, S. K.; Wozny, C. E. *J. Chem. Phys.* **1990**, *94*, 2817.
(14) Le Quéré, F.; Gray, S. K. *J. Chem. Phys.* **1993**, *98*, 5396.
(15) Roncero, O.; Halberstadt, N.; Beswick, J. A. *Chem. Phys. Lett.* **1994**, *226*, 82.
(16) Fang, J.-Y.; Guo, H. *J. Chem. Phys.* **1995**, *102*, 1944.
(17) García-Vela, A. *J. Chem. Phys.* **1996**, *104*, 1047.
(18) Moszynski, R.; Wormer, P. E. S.; van der Avoird, A. *J. Chem. Phys.* **1995**, *102*, 8385.
(19) Heijmen, T. G. A.; Moszynski, R.; Wormer, P. E. S.; van der Avoird, A.; Buck, U.; Steinbach, C.; Hutson, J. M. *J. Chem. Phys.* **1998**, *108*, 4849.
(20) Nejad-Sattari, M.; Stephenson, T. A. *J. Chem. Phys.* **1997**, *106*, 5454.
(21) Stephenson, T. A.; Halberstadt, N. *J. Chem. Phys.* **2000**, *112*, 2265.
(22) Burroughs, A.; Heaven, M. C. *J. Chem. Phys.* **2001**, *114*, 7027.
(23) Burroughs, A.; Kerenskaya, G.; Heaven, M. C. *J. Chem. Phys.* **2001**, *115*, 784.
(24) Boucher, D. S.; Bradke, M. D.; Darr, J. P.; Loomis, R. A. *J. Phys. Chem. A* **2003**, *107*, 6901.
(25) Gerber, R. B.; Buch, V.; Ratner, M. A. *J. Chem. Phys.* **1982**, *77*, 3022.
(26) Schatz, G. C.; Buch, V.; Ratner, M. A.; Gerber, R. B. *J. Chem. Phys.* **1983**, *79*, 1808.
(27) Bisseling, R.; Kosloff, R.; Gerber, R. B.; Ratner, M. A.; Gibson, L.; Cerjan, C. *J. Chem. Phys.* **1987**, *87*, 2760.
(28) Alimi, R.; Gerber, R. B.; Hammerich, A. D.; Kosloff, R.; Ratner, M. A. *J. Chem. Phys.* **1990**, *93*, 6484.
(29) Darr, J. P.; Loomis, R. A.; McCoy, A. B. *J. Chem. Phys.* **2005**, *122*, 044318.
(30) Cabrera, J. A.; Bieler, C. R.; Olbricht, B. C.; van der Veer, W. E.; Janda, K. C. *J. Chem. Phys.* **2005**, *123*, 054311.
(31) García-Vela, A.; Janda, K. C. *J. Chem. Phys.* **2006**, *124*, 034305.
(32) García-Vela, A. *J. Chem. Phys.* **2007**, *126*, 124306.
(33) García-Vela, A. *J. Chem. Phys.* **2008**, *129*, 094307.
(34) Tusa, J.; Sulkes, M.; Rice, S. A. *Proc. Natl. Acad. Sci. U.S.A.* **1980**, *77*, 2367.
(35) Cerjan, C.; Rice, S. A. *J. Chem. Phys.* **1983**, *78*, 4952.
(36) Gray, S. K.; Rice, S. A. *J. Chem. Phys.* **1985**, *83*, 2818.
(37) Cabanillas-Vidosa, I.; Pino, G. A.; Rinaldi, C. A.; Ferrero, J. C. *Chem. Phys. Lett.* **2006**, *429*, 27.
(38) Cabanillas-Vidosa, I.; Rinaldi, C. A.; Pino, G. A.; Ferrero, J. C. *J. Chem. Phys.* **2008**, *129*, 144303.
(39) García-Vela, A. *J. Phys. Chem. A* **2006**, *110*, 8023.
(40) García-Vela, A. *J. Chem. Phys.* **2005**, *123*, 124311.
(41) Valdés, A.; Prosmiti, R.; Villarreal, P.; Delgado-Barrio, G.; Werner, H.-J. *J. Chem. Phys.* **2007**, *126*, 204301.
(42) Blazy, J. A.; Dekoven, B. M.; Russell, T. D.; Levy, D. H. *J. Chem. Phys.* **1980**, *72*, 2439.
(43) Sharfin, W.; Kroger, K.; Wallace, S. C. *Chem. Phys. Lett.* **1982**, *85*, 81.
(44) Dai, J.; Zhang, J. Z. H. *J. Chem. Phys.* **1996**, *104*, 3664.

JP8106759